Ocean Engineering 55 (2012) 101–115

Contents lists available at SciVerse ScienceDirect

Ocean Engineering

journal homepage: www.elsevier.com/locate/oceaneng

Mathematical modelling of forces acting on ships during lightering operations

Evert Lataire [a,*], Marc Vantorre [a], Guillaume Delefortrie [b], Maxim Candries [a]

[a] Ghent University, Maritime Technology Division, Technologiepark 904, 9052 Ghent, Belgium
[b] Flanders Hydraulics Research, Berchemlei 115, 2140 Antwerp, Belgium

ARTICLE INFO

Article history:
Received 6 February 2012
Accepted 21 July 2012
Available online 23 August 2012

Keywords:
Lightering
Ship-to-ship interaction
Mathematical model
Cargo transfer
Model tests

ABSTRACT

The transfer of liquid cargo (crude oil and LNG) from a larger ship (the ship to be lightered, STBL) to a smaller vessel (service ship) when both ships are moored to each other and sail at a (slow) constant forward speed is known as lightering. These ship to ship operations are expected to increase in the near future and are expected to take place in harsher environmental conditions (polar regions). In order to better understand the hydrodynamic phenomena involved in this specific manoeuvre, a knowledge-building project with user involvement entitled "Investigating Hydrodynamic Aspects and Control Strategies for Ship-to-Ship Operations" was carried out in 2007–2011. As a part of this project, more than two thousand captive model tests were carried out at the towing tank for manoeuvres in shallow water (co-operation Flanders Hydraulics Research — Ghent University) in Antwerp, Belgium. A model of a very large crude oil carrier (VLCC) was attached to the main frame of the towing carriage and a model of an Aframax tanker was attached to the computer controlled planar motion carriage. Forces, moments and vertical positions were measured on both models.

This paper covers the analysis of the extensive model test data reported by Lataire et al. (2009a) and the influence of different parameters on the manoeuvre. Particular attention is paid to the forces and moments induced on the service ship by the proximity of the ship to be lightered. A mathematical model of lightering manoeuvres for both the service ship and the ship to be lightered is derived. This model can be implemented in a ship manoeuvring simulator for training purposes.

1. Introduction

Larger ship dimensions have economical advantages for most parties involved in maritime transport but meet with restrictions when calling at ports or when navigating in shallow or restricted waters. Fully loaded ultra and very large crude oil carriers (ULCC, VLCC) can only reach harbours if the access channels have a sufficient width and depth. For different reasons, among which safety and environmental issues, recent years have seen an increase in lightering operations, which involves the transfer of cargo, in particular oil or liquefied gases, mostly from large vessels to smaller vessels which can deliver the cargo ashore.

In deep water, a standard lightering manoeuvre takes place with the *ship to be lightered* (*STBL*), typically a VLCC (of about 300,000 DWT), advancing on a straight course at a low, constant speed. The *service ship*, typically an Aframax type tanker (of about 100,000 DWT) initiates the lightering manoeuvre when sailing abreast of the STBL with approximately the same heading and forward speed at a lateral distance of about 200 m from the STBL. The Aframax makes a slow lateral approach towards the STBL with a minimal difference in heading. When the ships are side-by-side, floating pneumatic fenders act as energy absorbers. They play an important safety role and Sakakibara et al. (2011) developed a monitoring system of the internal pressure in the fenders. When the cargo transfer is completed, the service ship is detached and in the final phase of the lightering manoeuvre increases the forward speed slightly. Throughout the lightering manoeuvre, the (much larger) STBL keeps her course and speed constant. In this respect, lightering is similar to replenishment at sea (RAS) operation carried out by warships. The latter however, is only a limited (in cargo and time) transfer between two ships and the lateral distance between both ships is significantly larger compared to lightering.

Lightering operations have been carried out by trained mooring masters for more than 30 years (Hayden, 2011) but systems have been developed to assist with the operation. Pedersen et al. (2008) discuss how these systems measure intra-ship distance based either on the principles of a frequency modulated

* Corresponding author. Tel.: +32 9 264 55 57; fax: +32 9 264 58 43.
E-mail addresses: Evert.Lataire@UGent.be (E. Lataire), Marc.Vantorre@UGent.be (M. Vantorre), Guillaume.Delefortrie@mow.vlaanderen.be (G. Delefortrie), Maxim.Candries@UGent.be (M. Candries).

0029-8018/$ - see front matter © 2012 Elsevier Ltd. All rights reserved.
http://dx.doi.org/10.1016/j.oceaneng.2012.07.029

Nomenclature

B	[m] beam of the ship
c_{Nsym}	[-] coefficient of the mathematical model
c_{Nasym}	[-] coefficient of the mathematical model
c_T	[-] coefficient of the mathematical model
c_{Xmax}	[-] coefficient of the mathematical model
c_y	[-] coefficient of the mathematical model
c_{Ymax}	[-] coefficient of the mathematical model
c_ξ	[-] coefficient of the mathematical model
F_{NR}	[N] rudder normal force
F_{TR}	[N] rudder tangential force
g	[m/s^2] earth's gravity acceleration
h	[m] water depth
L_{PP}	[m] length between perpendiculars
K	[Nm] roll moment
N	[Nm] yaw moment
n	[rpm] propeller rate
Q_P	[N mm] torque on the propeller shaft
Q_R	[N mm] torque on the rudder shaft
T_A	[m] draft aft (APP)
T_F	[m] draft fore (FPP)
T_M	[m] draft midship
T_P	[N] thrust of the propeller
UKC	[-] under keel clearance
V	[m/s] ship speed
X	[N] surge force
x_{cc}	[m] longitudinal distance between midships sections (>0 if midship service ship is ahead of STBL)
Y	[N] sway force
y_{bb}	[m] lateral distance between ship sides
y_{cb}	[m] lateral distance between own ship centre line and side of target ship
y_{cc}	[m] lateral distance between ship centre lines
z_A	[m] sinkage aft
z_F	[m] sinkage fore
δ	[°] rudder angle
Δ_{corr}	[-] correction term
ξ	[-] longitudinal distance between the ships' midships section x_{cc} divided by a reference ship length
ρ	[kg/m^3] density
∇	[m^3] displacement volume
ψ	[°] heading

Subscripts

SS	service ship
STBL	ship to be lightered
O	own ship
ref	reference
T	target ship
0	earth bound coordinate system

continuous wave or on the Global Navigational Satellite System (GNSS) in combination with fibre-optic gyroscopes. Shimizu and Pedersen (2011) propose a system using stereo vision to measure the relative distances, headings and speeds of the ships. In terms of implementation of these systems, Husjord et al. (2011) discuss how a user-centred design approach can be applied to develop a decision support system with a graphical user interface (GUI) that is appealing to mooring masters.

To safely carry out lightering operations, mooring masters are trained on a full mission bridge simulator. An accurate prediction of the forces and moments acting on both ships during a lightering manoeuvre is very important for the reliability of the simulation. The hydrodynamic interaction effects are expected to depend on the size and loading condition of the ships, the lateral and longitudinal separation distance between the ships, their speeds and underwater hull forms and the water depth.

Experimental work has been carried out to study the hydrodynamic interaction forces during lightering operations. Opheim (2005) and De Decker (2006) carried out captive model tests with the same models in the same facility but with a different experimental set-up. In both tests, the tanker models were free to heave and pitch but because of the use of a single towing carriage, the relative position of the ships during a single test run remained unchanged. Lataire et al. (2009a) carried out captive model tests of lightering manoeuvres in a shallow water towing tank, which are summarized in Section 2 of the paper. Yasukawa and Yoshida (2011) carried out captive model tests with two identical 1.2 m long Wigley hull forms towed at the same speed without stagger between them. Both ships were equipped with a rectangular type rudder model with a NACA0020 wing section and dynamometers were used to measure the hydrodynamic forces acting on the hulls and rudders. Tests were conducted at a Froude number of 0.165 for different drift angles, rudder angles and lateral distances.

Numerical methods have also been applied to study the hydrodynamic interaction effects which occur during lightering operations. Based on slender body theory, Tuck and Newman (1974) calculated the sway forces and yaw moments for two ships moving on parallel courses in deep water. The theory applies to two ships which are stationary relative to each other and when the flow is steady. Fang and Kim (1986) developed a strip theory method to predict the wave-induced motions on two closely spaced slender bodies advancing in oblique waves. This 2D method overestimates the interaction effects due to the wave energy trapping between the two hulls in the frequency range which is important for ship motions. Chen and Fang (2001) used a 3D source distribution technique to study the same problem and found that the 3D method is generally superior to the 2D method, particularly in the resonance region. Fang and Chen (2003) used systematic spectral analysis to find the significant amplitude of the relative motions obtained with the 3D method.

Skejic and Faltinsen (2007) developed a unified seakeeping and manoeuvring model for interacting ships intended for use in a real-time manoeuvring simulator. The hydrodynamic interaction between two ships is included in a module which is based on the far field slender body theory of Tuck and Newman (1974). To eliminate subjectivity, an autopilot is also included as a motion control module. Skejic and Berg (2009, 2010) used the unified seakeeping and manoeuvring model to study lightering operations between two tankers in calm water and in specified wave field conditions. It was found that the applied rudder angles were in qualitative agreement with the observed rudder angles during real lightering manoeuvres. In comparison to the situation in calm water, incident waves cause drifting motions and lead to greater collision risk, which should be accounted for by extra safety measures.

Xiang and Faltinsen (2010) extended the unified seakeeping and manoeuvring model for interacting ships developed by Skejic and Faltinsen (2007) by calculating the non-lifting dynamic hull loads accounting for ship interactions with a 3D potential flow method instead of using the far-field slender body theory. The advantage of this 3D method is that it allows for arbitrary relative configurations of the ships up to the point of collision. In addition, more than two ships and other interacting structures can be considered. The interaction model was compared with the experimental results of De Decker (2006) and good agreement was found.

This paper proposes an improved mathematical manoeuvring model for the surge force, the sway force and the yaw moment during a lightering manoeuvre both for the service ship and the STBL. The model is based on the experimental data of Lataire et al. (2009a), and does not include response to waves. The need for such a model was discussed by Lataire et al. (2011), who attempted to extrapolate the mathematical models for ship-ship interaction forces during meeting and overtaking developed by Vantorre et al. (2002) to lightering manoeuvres but found that the extrapolation to a zero longitudinal speed difference between the two vessels in proximity does not lead to good results. The experiments of Lataire et al. (2009a) are summarized in Section 2 and thoroughly analysed in Section 3. Particular attention is paid to the influence of different parameters on the manoeuvrability of the service ship. Finally, the proposed improved mathematical model is described in Section 4.

2. Experimental program

2.1. Test facilities

The towing tank for manoeuvres in shallow water with main dimensions $88 \times 7 \times 0.5\ \mathrm{m}^3$, is equipped with a planar motion carriage (consisting of a longitudinal or main carriage, a lateral carriage and a yaw table), a wave generator and an auxiliary carriage for ship-to-ship interaction tests with two ship models sailing at different speeds (overtaking and meeting manoeuvres). Full computer control allows unmanned operation of the facilities so that experimental programs can run day and night, seven days a week (Van Kerkhove et al., 2009). The number of test runs is only limited by the time needed for the water to calm down in between runs. An average of 35 tests a day can be achieved.

For the lightering test program, the tank facility was adapted to enable the attachment of two ship models to the main carriage. The auxiliary carriage was not used in order to avoid any longitudinal speed differences with respect to the main carriage. The model of the service ship (Aframax type) was attached to the planar motion mechanism (PMM), while the ship to be lightered (VLCC) was mounted directly to the main carriage by means of a rigid Rose-Krieger construction (Fig. 1). This implies that the STBL can only perform a motion in the longitudinal direction of the tank, while the service ship can perform any motion in the horizontal plane applied by the PMM. Both models are free to heave and pitch but restricted with respect to the carriage mechanism in all other directions. All forces, moments and motions measured on both ship models are summarised in Table 1.

Furthermore three wave gauges were installed at a fixed position in the tank to register the wave pattern. One small wave gauge is installed between both ship models (#2 in Fig. 2), one at the port side of the STBL (#3 in Fig. 2) and one at the starboard side of the service ship (#1 in Fig. 2). The exact position of the wave gauges in the towing tank is given in Table 2 and the relevant coordinate system in Fig. 3.

2.2. Ship models

Two ship models are involved in the ship to ship interaction tests. The ship to be lightered is a model of a large crude oil carrier. The geometric properties of bare hull, propeller and rudder of this vessel are made available and published via SIMMAN (2008). This specific model is known as the KVLCC2 Moeri tanker and often used as a benchmark vessel by towing tanks worldwide (Stern and Agdrup, 2008). The service ship is an Aframax type of vessel of about 100,000 DWT. Both models are tested with the appendages rudder and propeller attached. The main properties of both vessels are summarised in Table 3 and the body plans are shown in Figs. 4 and 5.

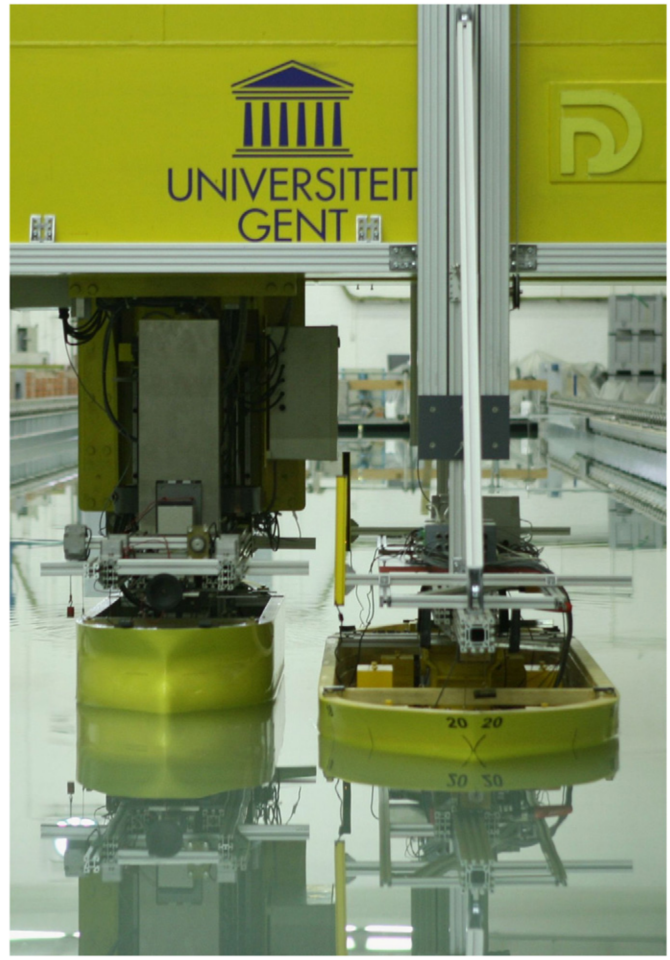

Fig. 1. Planar motion mechanism with the service ship attached (left) and the new construction with the ship to be lightered (right). Both are attached directly to the main carriage of the towing tank.

Table 1
Measured forces, moments and motions on service ship and ship to be lightered.

		Service ship	STBL	
Hull	Sinkage fore	$z_{F,SS}$	–	[m]
	Sinkage aft	$z_{A,SS}$	–	[m]
	Surge force	X_{SS}	X_{STBL}	[N]
	Sway force	Y_{SS}	Y_{STBL}	[N]
	Yaw moment	N_{SS}	N_{STBL}	[Nm]
	Roll moment	K_{SS}	–	[Nm]
Propeller	Propeller thrust	$T_{P,SS}$	$T_{P,STBL}$	[N]
	Propeller torque	$Q_{P,SS}$	$Q_{P,STBL}$	[Nm]
	Propeller rate	N_{SS}	n_{STBL}	[rpm]
Rudder	Rudder normal force	$F_{NR,SS}$	–	[N]
	Rudder tangential force	$F_{TR,SS}$	–	[N]
	Rudder torque	$Q_{R,SS}$	–	[Nm]
	Rudder angle	δ_{SS}	–	[deg]

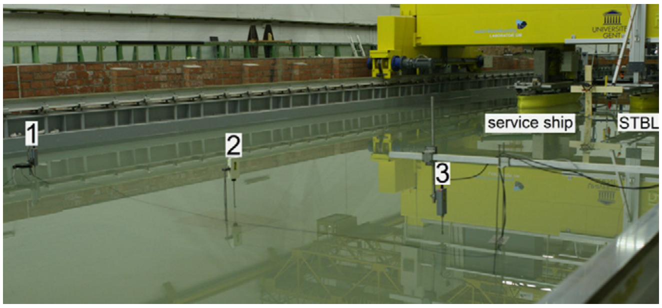

Fig. 2. The three wave gauges positioned at the same longitudinal position of the towing tank.

Table 2
Position of the wave gauges in the towing tank.

Wave gauge	x_0 [m]	y_0 [m]
1	50.00	−1.834
2	50.00	0.595
3	50.00	2.166

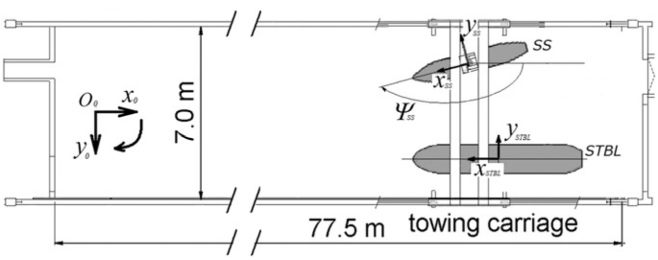

Fig. 3. Test setup and coordinate systems of importance.

Table 3
Main properties of both ship models on model scale and full scale.

	Service ship		STBL		
Scale	1	75	1	75	[-]
L_{PP}	231.4	3.085	320.0	4.267	[m]
B	42.0	0.560	58.0	0.773	[m]
	Design condition		**Design condition**		
T_F	15.0	0.200	20.8	0.277	[m]
T_M	15.0	0.200	20.8	0.277	[m]
T_A	15.0	0.200	20.8	0.277	[m]
∇	109,139	0.259	312,622	0.741	[m^3]
	Ballast condition		**2nd off load**		
T_F	7.5	0.100	12.8	0.171	[m]
T_M	8.3	0.111	12.8	0.171	[m]
T_A	9.1	0.121	12.8	0.171	[m]
∇	58,456	0.139	182,941	0.434	[m^3]

2.3. Model tests

Two types of tests were carried out during the test program: steady state tests and dynamic tests. During the regime condition of a steady state test the STBL and the service ship sail at the same speed and all parameters (rudder angle, propeller rate,…) of the models are kept constant. Three different types of dynamic tests were carried out: pure sway tests, pure yaw tests and varying rudder angle tests. During the first type the service ship moves along a sinusoidal path towards and away from the ship to be lightered while the ships' forward speeds and headings remain constant. A pure yaw test is analogous but the service ship performs a harmonic yawing motion. During the third type of dynamic test the rudder angle of the service ship harmonically varies as a function of time (from 40 degrees port to 40 degrees starboard and back) while the forward speed remains constant and the service ship does not yaw nor sway. The systematic test program comprised 1981 steady state tests and 162 dynamic tests.

Both ship models have been tested at two different drafts. The service ship has been tested in ballast condition and fully loaded while the STBL was either fully loaded or at even keel with a displacement corresponding with the condition after the second off load. Four combinations are possible; however, as both ships are never fully loaded simultaneously during a lightering manoeuvre in real life, this combination has not been tested.

The manoeuvres have been tested at two water depths; at 35.6 m full scale which is the practical maximal water depth of the shallow water towing tank at this scale and at an under keel clearance of 35% of the draft of the vessel with the deepest draft. Depending on the combination of loading conditions this can be the service ship or the VLCC. According to the present practice, lightering always takes place in deep water, so that the deep water condition can be considered as the most important one.

Tests have been carried out at forward speeds of 2.0, 4.0, 5.0 and 6.0 knots full scale. The propeller rate of the STBL always corresponded to the self-propulsion point (at model scale) at the design draft in open water i.e., without the influence of the service ship. The water depth during the self-propulsion tests with the STBL was always according to 35.6 m full scale while the self-propulsion of the service ship was tested at all combinations of draft (2) and water depth (2). During the model tests of a lightering manoeuvre the propeller rate of the service ship was

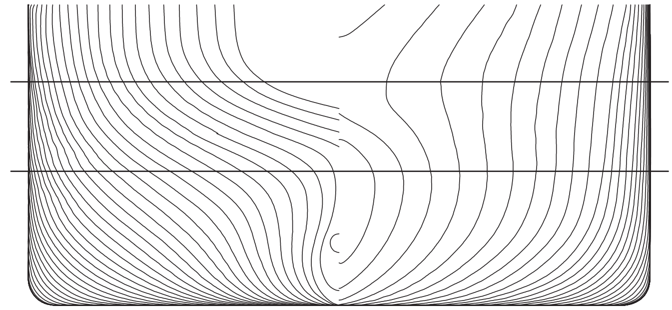

Fig. 4. Body plan of the ship to be lightered (STBL) including both water lines at the tested drafts.

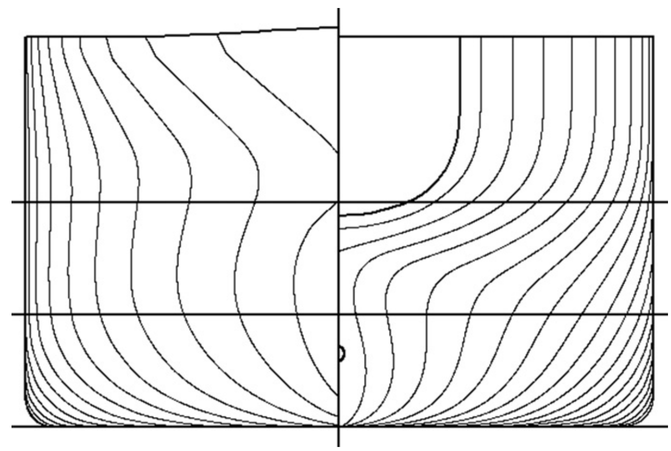

Fig. 5. Body plan of the service ship including both water lines at the forward perpendicular at the tested drafts.

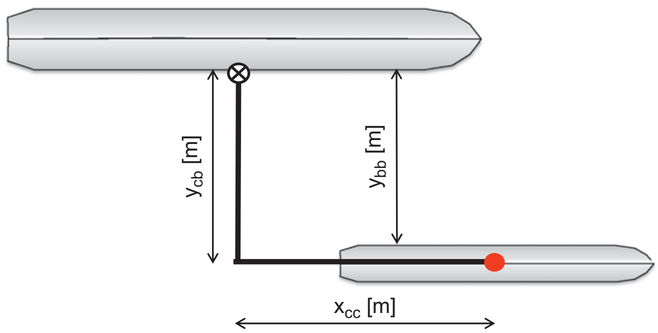

Fig. 6. Definition of the relative longitudinal position x_{cc} and the relative lateral position y_{cb}, in this figure both are positive.

according to self-propulsion (at the corresponding under keel clearance) and at telegraph positions *slow ahead* and *half ahead*.

The relative longitudinal as well as lateral positions were varied during the model tests, see Fig. 6. The relative longitudinal position is expressed by the distance x_{cc} between the midship sections of both vessels, x_{cc} being positive if the service ship is sailing ahead of the STBL. The lateral distance between both vessels is either expressed by the distance between ship's sides, y_{bb} or by the lateral distance between the centreline of the ship under analysis (or own ship) and the side of the target ship, y_{cb}. With B the beam of the own ship, the relationship between y_{cb} and y_{bb} can be written as:

$$y_{cb} = y_{bb} + \frac{B}{2} \tag{1}$$

The range of tested lateral and longitudinal positions of the service ship with respect to the STBL was selected taking account of the common practice of lightering manoeuvres. A standard lightering manoeuvre takes place with the relative longitudinal position around zero ($x_{cc} \approx 0$), as the manifolds for the oil transfer are located around the midship sections on both vessels. At a lateral distance of about 100 m, board to board, the service ship sails at the same heading and speed as the STBL. Slowly the service ship approaches the STBL with a very small relative heading until both vessels are moored to each other and with fenders of about 4 m diameter positioned in between both hulls, as shown in Fig. 7.

For training purposes, however, it is important to cope with a wider range of relative positions between both vessels other than the common positions during a standard lightering manoeuvre.

In all pure sway and yaw test runs, 100 m was taken as the initial position of the approach stage of the lightering manoeuvre of the service ship towards the STBL, while 4.0 m was taken as the clearance between both vessels when both are connected to each other, being a typical dimension for fenders. Five lateral distances between both vessels' sides have been tested systematically during steady state and dynamic rudder tests, i.e., y_{bb}=4.0, 10.0, 25.0, 50.0 and 100.0 m full scale. For a limited amount of tests, additional lateral positions have been tested, as indicated in Fig. 8.

Not only the lateral distance but also the relative longitudinal distance x_{cc} varies. Three longitudinal positions have been tested systematically: the midship sections of both vessels at the same relative longitudinal position $x_{cc}=0$, the STBL shifted ahead with a distance equal to half of the length of the service ship $x_{cc}=-Lpp_{SS}/2$ and the STBL shifted astern with a distance equal to half of the length of the service ship $x_{cc}=Lpp_{SS}/2$. For two lateral positions, a limited amount of tests were carried out with a wider range of relative longitudinal positions. The systematic combinations of relative lateral and longitudinal positions between both vessels are indicated by black dots in Fig. 8, whereas other positions which have not been tested systematically are indicated by circles.

Fig. 7. Picture (courtesy of Yunja Yoo, NTNU) taken from the service ship, the fenders in between both vessels clearly visible.

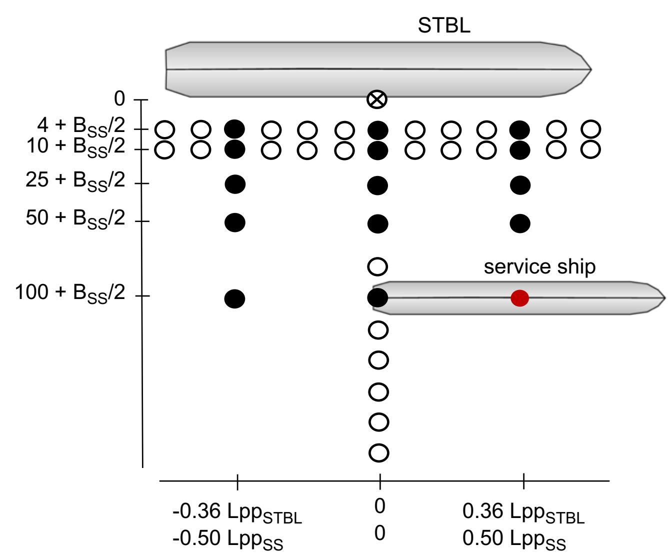

Fig. 8. All relative positions between both vessels tested, systematically (black dots) and limited (circles).

The last parameter to be varied is the relative heading. The STBL never had a drift angle while the service ship was tested with drift angles of 0.0, 1.0, 2.0, 3.0 and 5.0 degrees, mostly with her bow towards the STBL.

3. General aspects of ship-to-ship interaction forces

3.1. Pressure distribution

Unlike an overtaking manoeuvre, lightering can be interpreted as a quasi-steady process because of the rather slow approach of the service ship towards the STBL. Only in order to gain more

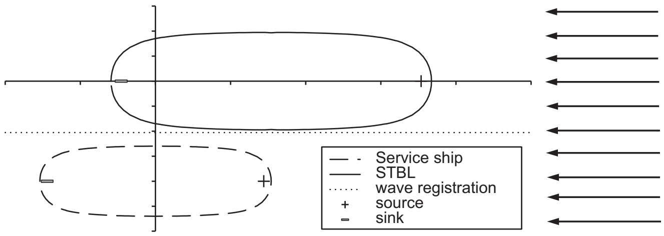

Fig. 9. Two dimensional potential flow with two Rankine ovals representing the STBL and service ship in a uniform flow.

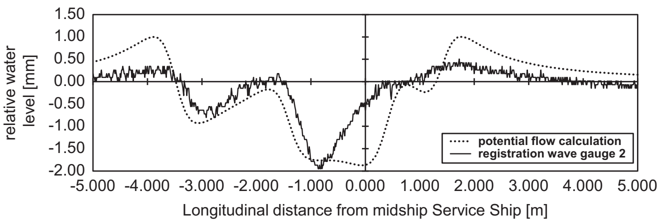

Fig. 10. Comparison between measured wave pattern and potential flow calculation (at model scale) for a lightering manoeuvre at full scale at 4.0 knots, $x_{cc}=Lpp_{SS}/2$, $y_{bb}=10.0$ m and a water depth of 35.6 m.

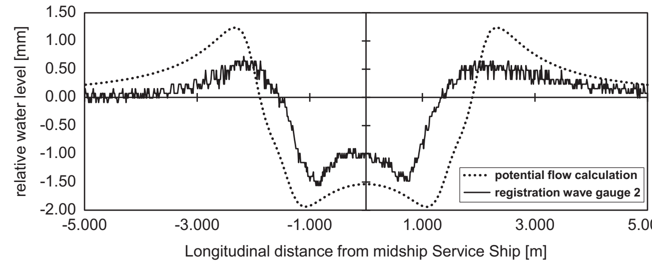

Fig. 11. Comparison between measured wave pattern and potential flow calculation (at model scale) for a lightering manoeuvre at full scale at 4.0 knots, $x_{cc}=0$, $y_{bb}=10.0$ m and a water depth of 35.6 m.

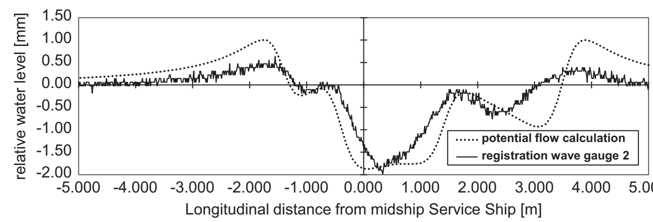

Fig. 12. Comparison between measured wave pattern and potential flow calculation (at model scale) for a lightering manoeuvre at full scale at 4.0 knots, $x_{cc}=Lpp_{SS}/2$, $y_{bb}=10.0$ m and a water depth of 35.6 m.

insight into the overall pressure distribution along the hull of both vessels, the hydrodynamically complex lightering manoeuvre is simplified according to the two dimensional potential flow theory. Each ship is represented by a dipole in a uniform flow. The magnitude m and relative distance $2a$ of the source and sink is such that the Rankine oval they produce in the uniform flow has the same length and width as the vessels' length and beam they represent. The influence of the ovals representing the service ship and STBL on the geometry of each other is small and therefore neglected.

In Fig. 9 the represented STBL is positioned ahead $x_{cc}=-Lpp_{SS}/2$ of the represented service ship at a distance $y_{bb}=10.0$ m between the ships' sides. The uniform flow is 4.0 knots full scale. The dotted line in the same figure is at the same lateral position from the ship sides as wave gauge 2 (Fig. 2) during the model tests.

Fig. 10 shows the free surface elevation determined with the two dimensional potential flow theory, compared with the measurements for the same condition as shown in Fig. 9. Taking into account the very simplified calculation method, the registered wave is qualitatively well predicted. The assumption of the undisturbed two dimensional superposition of a high pressure region around the bow section and a low pressure region around the stern section of each vessel seems to be valid based upon the wave registration. Based on the qualitatively good agreement between the computed and registered wave elevations, the numerical method can be expected to predict the forces and moments during a lightering operation relatively well.

Other comparisons between potential flow calculation and wave registration are shown for different relative longitudinal positions in Fig. 11 ($x_{cc}=0$) and Fig. 12 ($x_{cc}=Lpp_{SS}/2$).

3.2. Relative longitudinal position

The STBL will influence the service ship differently depending on the relative longitudinal position between the STBL and the service ship. For constant values of speed, water depth and lateral position y_{cb} but for a wide range of relative longitudinal positions x_{cc}, the influence of the STBL on the service ship is given for the surge force in Fig. 13, the sway force in Fig. 14 and the yaw moment in Fig. 16. In all these figures, the forces and moment are made dimensionless making use of positive reference values (X_{ref}, Y_{ref} and N_{ref}).

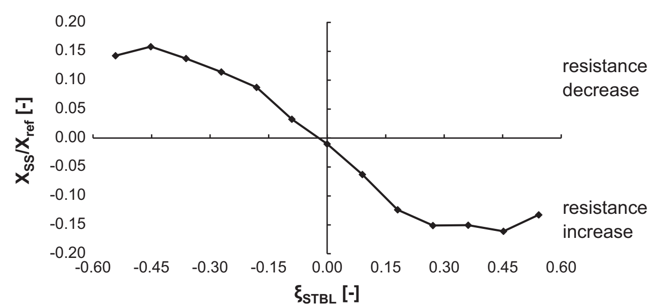

Fig. 13. Surge force on the service ship (made dimensionless via X_{ref}) induced by the proximity of the STBL with $y_{bb}=10.0$ m at 4.0 knots full scale for a wide range of ξ_{STBL} and a water depth of 35.6 m.

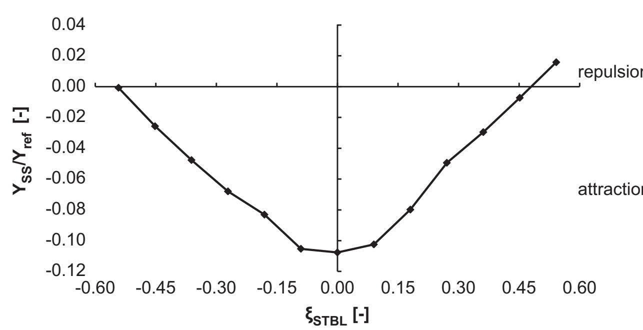

Fig. 14. Sway force on the service ship (made dimensionless via Y_{ref}) induced by the proximity of the STBL with $y_{bb}=10.0$ m at 4.0 knots full scale for a wide range of ξ_{STBL} and a water depth of 35.6 m.

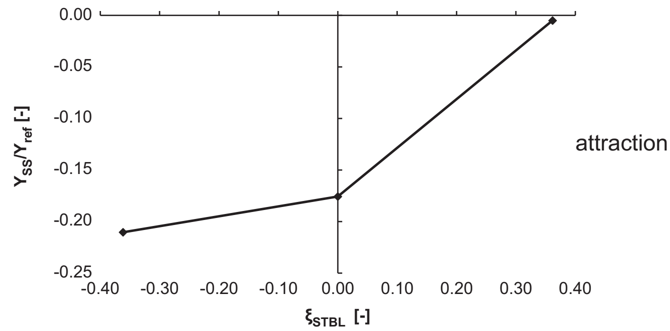

Fig. 15. Sway force on the service ship (made dimensionless via Y_{ref}) induced by the proximity of the STBL with $y_{bb}=10.0$ m at 4.0 knots full scale for three ξ_{STBL} and a water depth of 20.25 m (35% UKC_{SS}).

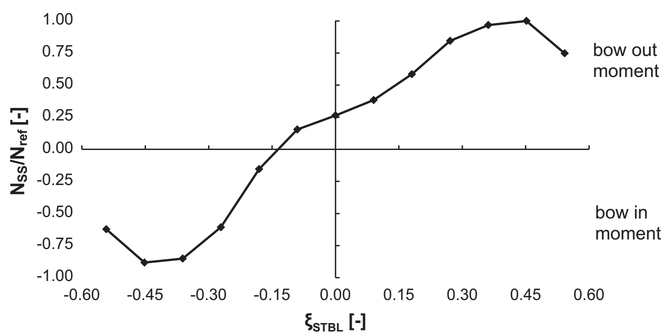

Fig. 16. Yaw moment (made dimensionless via the highest registered yaw moment in this condition N_{ref}) on the service ship induced by the proximity of the STBL with $y_{bb}=10.0$ m at 4.0 knots full scale for a wide range of ξ_{STBL} and a water depth of 35.6 m.

In Fig. 13 the dimensionless surge force is plotted to the dimensionless relative longitudinal position of both vessels ξ_{STBL}.

$$\xi_{STBL} = \frac{x_{cc}}{Lpp_{STBL}} \tag{2}$$

The influence on the surge force becomes negligible when both midship sections are at the same longitudinal position, but when the midship section of the service ship is aft of the midship section of the STBL ($\xi_{STBL} < 0$) the resistance of the service ship decreases. The service ship will be pushed forward by the proximity of the low pressure region around the stern of the STBL. When the service ship's midship is ahead of the STBL's midship ($\xi_{STBL} > 0$) the resistance of the service ship will increase, causing a deceleration of the vessel. Although Fig. 13 shows X_{SS}/X_{ref} only for one UKC, one speed and one lateral position y_{bb} (at a propeller rate which is self-propulsion in open water) the same qualitative results are obtained at other UKC's, speeds and lateral positions.

As postulated in Section 3.1, the complex hydrodynamics during a lightering manoeuvre can be interpreted qualitatively with potential flow theory. The section between both ship sides suffers from higher water velocities than the sections at the outer side, which results in a pressure distribution along the hull being lower in between both vessels than at their outer sides. This pressure distribution results in a sway force directed towards the other vessel, so both vessels will be attracted to each other. Fig. 14 shows a maximal attraction of the service ship towards the STBL when both midships are at the same longitudinal position ($\xi_{STBL} \approx 0$). In this situation the water between both ship sides accelerates along the entire hull and generates the highest sway force; the latter decreases when both ship sides overlap less, since the fraction of the ship lengths affected by accelerated flow decreases with increasing $|\xi_{STBL}|$ values.

This observation is qualitatively valid for all speeds and lateral positions but not for all UKC's. When both ships sail in shallow water the symmetry for the service ship sailing fore or aft the STBL disappears. The magnitude of the sway force at negative ξ_{STBL} values increases, as shown in Fig. 15. The service ship is attracted more towards the STBL when the STBL is ahead of the service ship than when both midships are at the same longitudinal position or the service ship is ahead of the STBL. The effect of UKC will be discussed in more detail in Section 3.4.

The yaw moment on the service ship induced by the proximity of the STBL for a range of longitudinal positions ξ_{STBL} is shown in Fig. 16. When the stern of the STBL is ahead the service ship ($\xi_{STBL} < -0.14$) the yaw moment on the service ship is negative, which implies that the bow of the service ship will be attracted towards the STBL. When the service ship is ahead of the STBL, the yaw moment is positive or the bow of the service ship is pushed away from the STBL while her stern is attracted towards the STBL.

As mentioned in Section 2.3, most lightering operations take place with both midships at about the same longitudinal position. According to Figs. 13 and 14, this can be considered as the most appropriate longitudinal position in that the interaction will have the least influence on the surge force, while the lateral attraction force will be beneficial during the lightering operation. In real life the latter is recognised by the lightering pilots who use the lateral force to their advantage when piloting the service ship towards the STBL. However, sometimes this sway force hinders a smooth separation of the vessels when the cargo transfer is terminated.

3.3. *Relative lateral position*

Not only the relative longitudinal distance but also the lateral distance between both ships will change the degree of the hydrodynamic influence of both vessels on each other. Fig. 17 shows the magnitude of the surge force on the service ship at a forward speed of 4.0 knots. The absolute value of the surge force decreases with an increasing distance between both vessels. The influence on the surge force when both vessels' midship sections are at the same longitudinal position is almost unchanged and close to zero.

For the same test conditions as for Fig. 17, the sway force on the service ship is shown in Fig. 18. This sway force also increases with a decreasing lateral distance y_{cb} between both vessels for all longitudinal positions. It may be noted that the attraction (negative values) becomes a repulsion force away from the STBL at high y_{cb} values (or low B_{SS}/y_{cb} ratio). This force is not induced by the STBL but by the close proximity of the wall of the towing tank at the starboard side of the service ship. The bank effect induces an

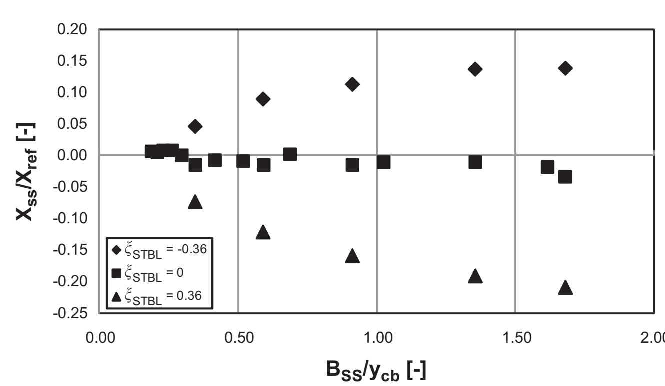

Fig. 17. Surge force on the service ship induced by the proximity of the VLCC at 4.0 knots full scale for a wide range of lateral distances y_{cb} and three relative longitudinal distances ξ_{STBL} and a water depth of 35.6 m.

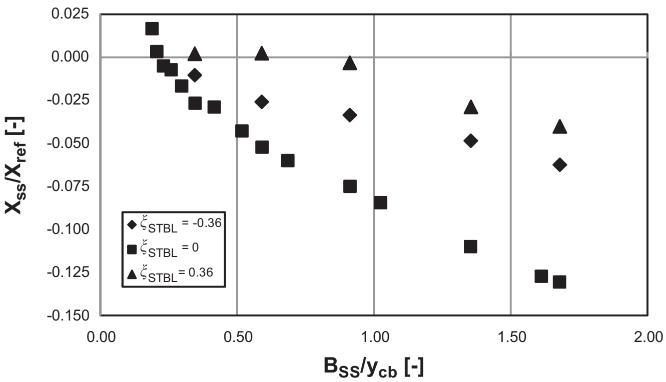

Fig. 18. sway force on the service ship induced by the proximity of the VLCC at 4.0 knots full scale for a wide range of lateral distances y_{cb} and three relative longitudinal distances ξ_{STBL} and a water depth of 35.6 m.

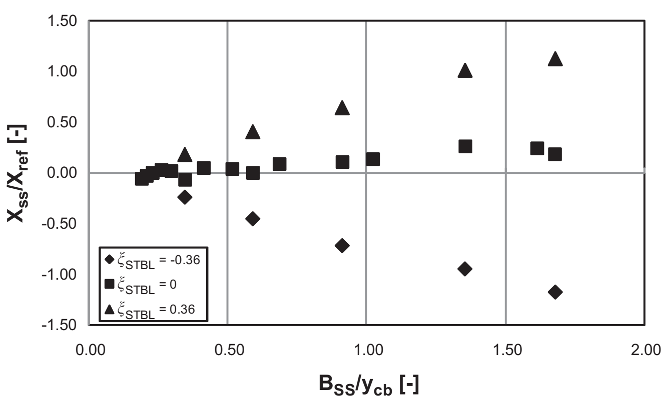

Fig. 19. Yaw moment on the service ship induced by the proximity of the VLCC at 4.0 knots full scale for a wide range of lateral distances y_{cb} and three longitudinal distances and a water depth of 35.6 m.

attraction force on the service ship resulting in a positive sway force (Lataire et al., 2009b).

The yaw moment induced on the service ship by the STBL when both sail at 4.0 knots for three relative longitudinal positions and a wide range of lateral positions is shown in Fig. 19. The magnitude of the yaw moment decreases when the lateral distance between both ships increases. This is valid for the three relative longitudinal positions shown in Fig. 19. The (small) negative yaw moment at the highest y_{cb} values tested is again ascribed to the bank effects induced by the wall of the towing tank.

3.4. Draft and under keel clearance of the service ship

The loading condition of both ships varies during the lightering operation. Initially the STBL is fully loaded and the approaching service ship sails in ballast condition. When both ships separate the service ship is fully loaded and the STBL is less than fully loaded. A second ballasted service ship can now approach and continue to lighter this STBL. As shown in Table 3 the service ship and the STBL were both tested at two different loading conditions. Most lightering manoeuvres take place in (very) deep water but tests have been carried out at different water levels to study possible shallow water effects. All tested combinations of drafts of both vessels and water depths are summarised in Table 4 together with the UKC for the service ship and STBL.

In Fig. 20 the surge force acting on the service ship is shown for three different longitudinal positions and for all tested water depths (2) and drafts of the service ship (2) with the STBL's draft at 12.8 m. In this case at 6.0 knots full scale, with 10 m between both ship sides (y_{bb}) and with a propeller rate according to self-propulsion in open water. The absolute value of the surge force decreases when the under keel clearance of the service ship increases or when more water can flow unrestricted under the ship's hull.

For the same test conditions as in Fig. 20 the yaw moment N_{SS} induced by the vicinity of the STBL for different water depths is plotted in Fig. 21. The magnitude of the yaw moment decreases for an increasing T_{SS}/h ratio. As mentioned, the influence of the water depth on the magnitude of the sway force varies for different longitudinal positions. Fig. 22 shows the sway force of the service ship for three different longitudinal positions and at four different water depths. When the water is deep enough (i.e., UKC values of more than 0.90), the magnitude of the attraction force peaks when both midships are at the same longitudinal position. When both midships (both fore and aft) are separated by a significant relative longitudinal distance this attraction is much smaller. When the service ship is behind the STBL the vessel is

Table 4
Tested full scale water depth, draft, displacements and under keel clearances.

Water depth [m]	$T_{A,\,SS}$ **[m]**	$T_{A,\,STBL}$ **[m]**	∇_{SS} **[10^3m^3]**	∇_{STBL} **[10^3m^3]**	$T_{SS}/(h-T_{SS})$ **[-]**	$T_{STBL}/(h-T_{STBL})$ **[-]**
35.6	15.0	12.8	109.1	182.9	0.7	0.56
20.3	15.0	12.8	109.1	182.9	2.86	1.72
35.6	9.1	12.8	584.6	182.9	0.34	0.56
17.3	9.1	12.8	584.6	182.9	1.11	2.86
35.6	9.1	20.8	584.6	312.6	0.34	1.40
28.1	9.1	20.8	584.6	312.6	0.48	2.86

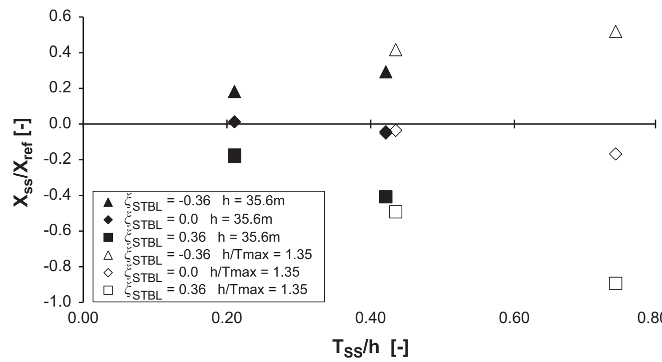

Fig. 20. Surge force on the service ship for different UKC_{SS} (with T_{STBL}=12.8 m; y_{bb}=10 m; at 6.0 knots and propeller rate according to self-propulsion).

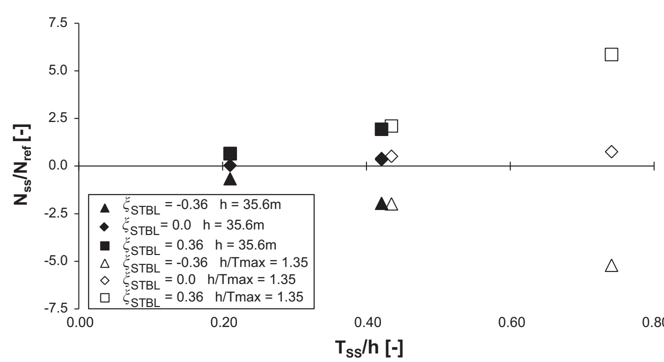

Fig. 21. Yaw moment on the service ship for different UKC_{SS} (with T_{STBL}=12.8 m; y_{bb}=10 m; at 6.0 knots and propeller rate according to self-propulsion).

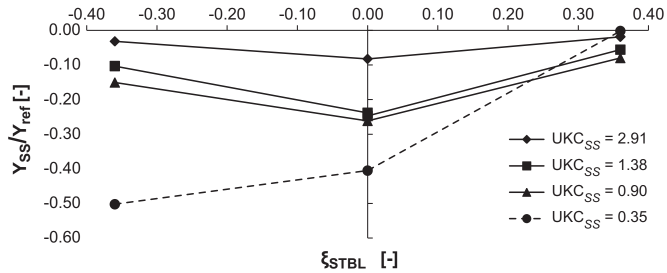

Fig. 22. Sway force on the service ship for different UKC_{SS} and relative longitudinal positions (with T_{STBL}=12.8 m; y_{bb}=10 m; at 6.0 knots and propeller rate according to self-propulsion).

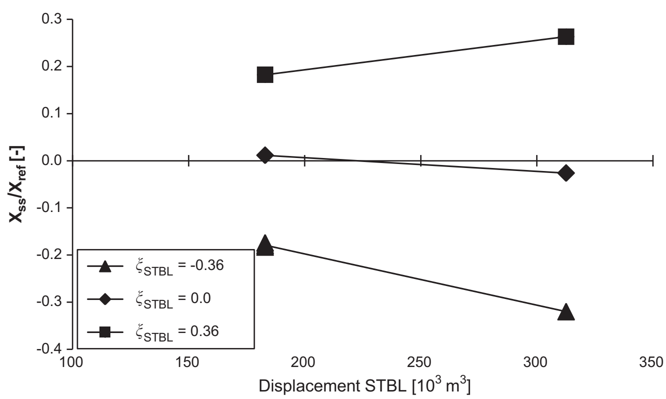

Fig. 23. Surge force measured on the service ship (made dimensionless with the positive value X_{ref}) in ballast condition and with the STBL in both tested volume displacements (with y_{bb}=10 m; at 6.0 knots and propeller rate according to self-propulsion and a water depth of 35.6 m).

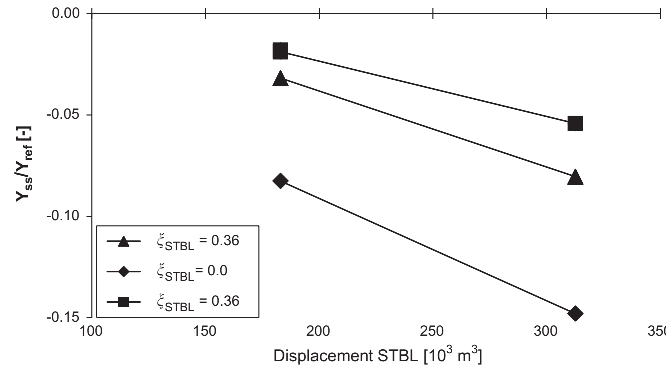

Fig. 24. Sway force measured on the service ship (made dimensionless with the positive value Y_{ref}) in ballast condition and with the STBL in both tested volume displacements (with y_{bb}=10 m; at 6.0 knots and propeller rate according to self-propulsion and a water depth of 35.6 m).

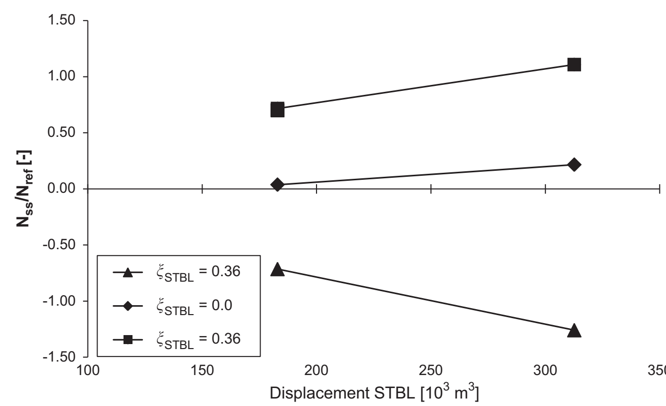

Fig. 25. Yaw moment measured on the service ship (made dimensionless with the positive value N_{ref}) in ballast condition and with the STBL in both tested volume displacements (with y_{bb}=10 m; at 6.0 knots and propeller rate according to self-propulsion and a water depth of 35.6 m).

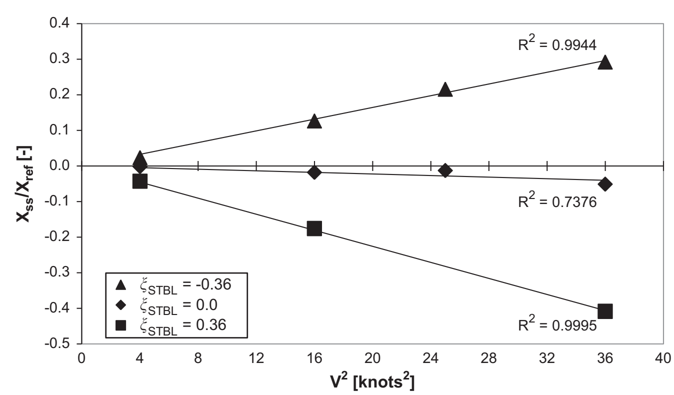

Fig. 26. Relative surge force on the service ship for different speeds (with T_{SS}=15.0 m; T_{STBL}=12.8 m; h=35.6 m; y_{bb}=10 m and propeller rate according to self-propulsion).

(slightly) more attracted towards the STBL with decreasing water depths. At very low water depths (UKC_{SS}=0.35) this is very explicit, the magnitude of the sway force is larger than in the situation when both midships are at the same longitudinal position.

Overall it can be concluded that at constant water depth, the forces and moments induced by the vicinity of a ship in close proximity increase with increasing draft of the service ship. An increasing water depth (or UKC) decreases all the forces and moments induced by the vicinity of a ship in close proximity.

3.5. *Loading condition of the STBL*

The displacement of the STBL has a significant influence on the magnitude of the forces induced on the service ship. The more water displaced, the more the streamlines around the service ship will be disturbed and the higher the magnitudes of the peak values are during the lightering manoeuvre. This is valid for the surge force (Fig. 23), the sway force (Fig. 24) and the yaw moment (Fig. 25).

3.6. *Forward speed*

For one specific test condition the relation between the surge force, yaw moment and sway force and the square of the forward speed is shown in Figs. 26, 27 and 28, respectively, for three relative longitudinal positions between the vessels. The tests shown in these figures are carried out with a water depth corresponding to a full scale water depth of 35.6 m, the service ship at design draft of 15.0 m and the STBL with a draft of 12.8 m. A constant lateral distance of y_{bb}=10.0 m was maintained and both vessels sailed with a propeller rate corresponding to the self-propulsion point (for each speed) in open water.

As known from literature, the magnitude of the surge and sway forces induced by the STBL on the service ship increases approximately linearly with the square of the forward speed, as shown in Figs. 26 and 27, respectively. The bow out and bow in moment on the service ship also increase quadratically with an increasing forward speed of both vessels, as illustrated in Fig. 28.

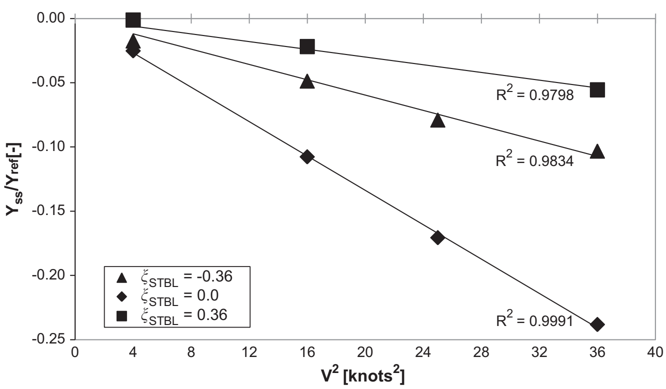

Fig. 27. Relative sway force on the service ship for different speeds (with $T_{SS}=15.0$ m; $T_{STBL}=12.8$ m; $h=35.6$ m; $y_{bb}=10$ m and propeller rate according to self-propulsion).

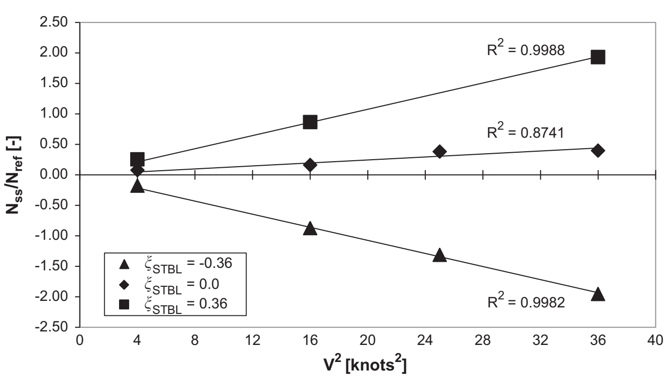

Fig. 28. Relative yaw moment on the service ship for different speeds (with $T_{SS}=15.0$ m; $T_{STBL}=12.8$ m; $h=35.6$ m; $y_{bb}=10$ m and propeller rate according to self-propulsion).

4. Mathematical model for lightering manoeuvres

A mathematical model is proposed for the surge force, sway force and yaw moment induced by the vicinity of a ship in close proximity and sailing at the same speed and heading as the ship under consideration. The model is based upon the previously described model tests and copes with a wide range of relative longitudinal and lateral positions between the vessels, loading conditions and forward speeds. The proposed mathematical model is based on the model tests performed with the highest possible water level in the towing tank, and is therefore only valid in deep water. In practice, this is the most important condition, as lightering always takes place in deep water. The effect of water depth on the surge force, sway force and yawing moment has been discussed in Section 3.4.

While the sway force Y takes an extreme value around $\xi_{STBL}=0$, the magnitude of the surge force X and moment N for this relative longitudinal position is small compared to their respective peak values. Nevertheless, because of the importance of X and N on the manoeuvre they cannot be ignored, even if their values are rather limited. In the proposed new mathematical model the extremes will be modelled and a predefined function will solve the results for the values between these calculated extremes.

4.1. Forces and moment on the service ship X_{SS}, Y_{SS}, N_{SS}

4.1.1. Surge force X_{SS}

When the midship of the service ship is more than half a ship length (of the service ship) fore or aft from the midship of the STBL ($|\xi_{STBL}| \approx 0.40$) then the influence on the surge force peaks (Fig. 13). The model is simplified in such way that the magnitude of the maximum increase of the surge force is as assumed equal to the maximum decrease (but with an opposite sign). First this peak value will be modelled based upon the model tests and then the model will be extended for all relative longitudinal positions.

The peak value for the change in surge force is modelled as follows ($c_T=1$):

$$X_{max} = c_{X_{max}} \frac{1}{2}\rho V^2 \frac{\nabla_{STBL}}{Lpp_{SS}} \left(\frac{T_{SS}}{B_{SS}}\right)^{c_T} \left(\frac{B_{SS}}{y_{cb}}\right)^{c_y} \quad (3)$$

This formula is only valid for the relative longitudinal position $\xi_{STBL}=0.40$ and is extended to cope with all relative longitudinal positions by:

$$X_{SS} = X_{max} \sin(c_\xi \pi \xi_{STBL}) e^{-\xi_{STBL}^2} \quad (4)$$

If the highest values occur at $|\xi_{STBL}|=0.40$ then c_ξ can be defined analytically.

$$\left.\frac{dX}{d\xi}\right|_{\xi=0.4} = \left.\frac{d(X_{max}\sin(c_\xi \pi \xi_{STBL}) e^{-\xi_{STBL}^2})}{d\xi}\right|_{\xi=0.4} = 0$$
$$\Rightarrow \quad c_\xi = 1.063 \quad (5)$$

As a simplification of Eq. (5) the constant c_ξ can be chosen to be exactly one, which shifts the peak of the surge force to $\xi_{STBL}=0.417$. The formula for the influence of the STBL on the surge force of the service ship is then:

$$X_{SS} = c_{X_{max}} \frac{1}{2}\rho V^2 \frac{\nabla_{STBL}}{Lpp_{SS}} \left(\frac{T_{SS}}{B_{SS}}\right)^{c_T} \left(\frac{B_{SS}}{y_{cb}}\right)^{c_y} \sin(\pi \xi_{STBL}) e^{-\xi_{STBL}^2} \quad (6)$$

Fig. 29 compares the experimental values with the results modeled with Eq. 6. Table 5 summarizes the main mathematical properties (an interval which contains the exact value of the parameter, the relative standard error and the relative lower and upper bound of the 95% confidence interval) of the regression for the three parameters.

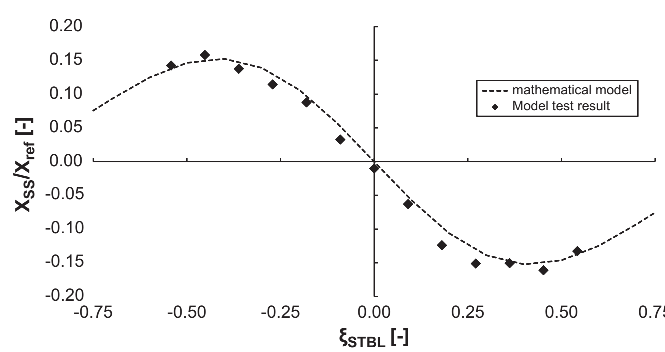

Fig. 29. Comparison between the measured surge force and the result of the mathematical model for a wide range of relative longitudinal positions between both vessels and with $y_{bb}=10.0$ m at 4.0 knots full scale and a water depth of 35.6 m.

Table 5
Parameter estimates for the mathematical model of the surge force on the service ship.

Parameter	Estimate	Std. error/ estimate	95% confidence interval	
			Lower bound/ estimate	Upper bound/ estimate
$C_{X_{max}}$	$-1 < C_{X_{max}} < 0$	-0.01	1.03	0.97
C_T	1	NA	NA	NA
C_Y	$0 < C_Y < 1$	0.05	0.90	1.10

$R^2 = 1-$(residual sum of squares)/(corrected sum of squares)$=0.964$.

4.1.2. Sway force Y_{SS}

Fig. 14 has shown that the sway force is characterized in deep water by a symmetric function with high attraction midships abeam.

The peak value of the sway force is modelled as follows ($c_y = 1$):

$$Y_{max} = c_{Y_{max}} \frac{1}{2} \rho V^2 \frac{\nabla_{STBL}}{Lpp_{SS}} \left(\frac{T_{SS}}{B_{SS}}\right)^{c_T} \left(\frac{B_{SS}}{y_{cb}}\right)^{c_y} \tag{7}$$

While the exact progression of the sway force for all relative longitudinal positions is modelled with a cosine:

$$Y_{SS} = Y_{max} \cos(c_\xi \pi \xi_{STBL}) e^{-(\xi_{STBL})^2} \tag{8}$$

Because the transition from an attraction force to a repulsion force takes place at $|\xi_{STBL}| \approx 0.40$, c_ξ can again be taken equal to 1 as shown for Eq. (5).

Combining Eqs. (7) and (8) results in:

$$Y_{SS} = c_{Y_{max}} \frac{1}{2} \rho V^2 \frac{\nabla_{STBL}}{Lpp_{SS}} \left(\frac{T_{SS}}{B_{SS}}\right)^{c_T} \left(\frac{B_{SS}}{y_{cb}}\right)^{c_y} \cos(c_\xi \pi \xi_{STBL}) e^{-\xi_{STBL}{}^2} \tag{9}$$

The proposed lightering model for the sway force, with the coefficient properties given in Table 6, can be compared with the measurements and a relative good comparison is found, as shown in Fig. 30.

4.1.3. Yaw moment N_{SS}

As shown in Fig. 16 the yaw moment is not point symmetric for the relative longitudinal position. Furthermore the most common longitudinal position during lightering is when both midships are at about the same longitudinal position. Therefore the yaw moment for ξ-values around zero has to be modelled very accurately.

The proposed mathematical model of the yaw moment is based upon the superposition of a point symmetric function around the origin (ξ and yaw moment are zero) and a function coping with the deviation from this point symmetry.

First the longitudinal position (ξ_{STBL}) and peak values of the magnitude of the yaw moment are determined. Based upon the systematic series of the longitudinal positions (a selection of this series is shown in Fig. 16) the longitudinal position, where the magnitude of the yaw moment peaks, is also at about $|\xi_{STBL}| = 0.40$. The maximal bow in moment $-N_{max}$ (at $\xi_{STBL} = -0.40$) is considered to have the same magnitude as the maximal bow out moment N_{max} (at $\xi_{STBL} = 0.40$) but with opposite sign. This peak in the yaw moment is modelled as follows:

$$N_{max} = c_{N_{max}} \frac{1}{2} \rho V^2 \frac{\nabla_{STBL}}{y_{cb}} \left(\frac{T_{SS}}{B_{SS}}\right)^{c_T} \tag{10}$$

To cope with a wide range of relative longitudinal positions this formula is extended by multiplying with an exponential decreasing sine:

$$N_{sym} = N_{max} \sin(c_\xi \pi \xi_{STBL}) e^{-\xi_{STBL}^2} \tag{11}$$

Again c_ξ can be defined analytically, cf. Eq. 5, provided that the highest values occur at $|\xi_{STBL}| = 0.40$ and this will again give $c_\xi = 1.063$. In this formula c_ξ will also be simplified to exactly one so the peak of the yaw moment shifts to $\xi_{STBL} = 0.417$.

In Fig. 31 the point symmetric model for the yaw moment and the measured yaw moment on the service ship are shown. The biggest deviation between the symmetric model and the measurements take place in the most important region for lightering (at small ξ_{STBL} values). Therefore a second formulation is added to this point symmetric formula.

For one test condition but at a wide range of longitudinal positions the deviation between the symmetric model and the measured yaw moments is shown in Fig. 32.

Table 6
Parameter estimates for the mathematical model of the sway force on the service ship.

Parameter	Estimate	Std. error/ estimate	95% confidence interval	
			Lower bound/ estimate	Upper bound/ estimate
$C_{Y_{max}}$	$-10 < C_{Y_{max}} < 0$	-0.07	1.13	0.87
C_T	$0 < C_T < 10$	0.03	0.93	1.07
C_Y	1	NA	NA	NA
C_ξ	1	NA	NA	NA

$R^2 = 1-$(residual sum of squares)/(corrected sum of squares)$=0.948$.

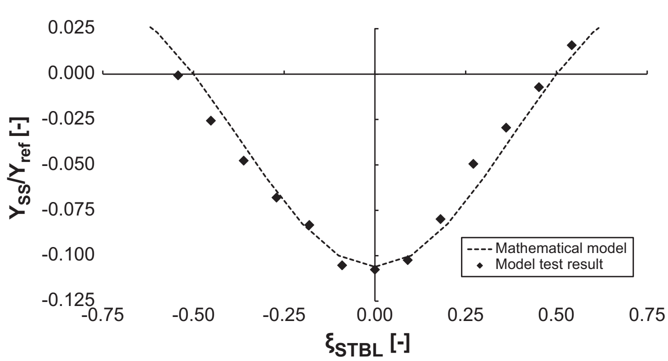

Fig. 30. Comparison between the measured and modelled sway force for a wide range of relative longitudinal positions between both vessels and with $y_{bb} = 10.0$ m at 4.0 knots full scale and a water depth of 35.6 m.

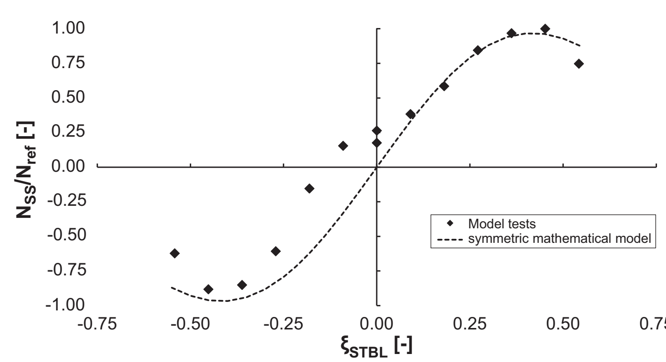

Fig. 31. Comparison between the measured yaw moment during model tests and the symmetric mathematical model for a wide range of relative longitudinal positions between both vessels and with $y_{bb} = 10.0$ m at 4.0 knots full scale and a water depth of 35.6 m.

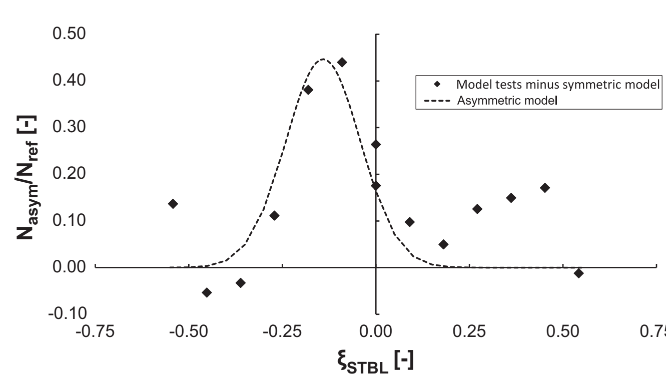

Fig. 32. Difference between measured yaw moment and point symmetric model.

This difference from the point symmetric model is modelled as a Gaussian function:

$$N_{asym} = c_{N_{asym}} \times e^{-(c_{N1}+c_{N2}\xi)^2} \quad (12)$$

$c_{N_{asym}}$ is the maximal deviation from the point symmetry as shown in Fig. 32 and in the other tested conditions at a relative longitudinal position ξ_{STBL} of about -0.14. At this relative longitudinal position the aft perpendicular of both vessels are at the same longitudinal position. This might help to understand the physics involved in the induced yaw moment. The streamlines around both vessels are squeezed in the aft ship region. When both regions interfere they will influence this higher order yaw moment.

$$\xi_{\mathrm{STBL}} = -\frac{Lpp_{\mathrm{STBL}} - Lpp_{SS}}{2Lpp_{\mathrm{STBL}}} = -0.14 \quad (13)$$

Only for a limited amount of tests a wide range of longitudinal positions was covered. Systematic tests were carried out at ξ_{STBL} values of -0.36; 0.0; 0.36. As a result the influence of the asymmetry has only been tested systematically at $\xi_{\mathrm{STBL}}=0.0$. Therefore the variance or the measure of the width of the distribution should be defined based upon the systematic tests with a wide range of longitudinal positions. So the (fixed) values for c_{N1} and c_{N2} become:

Peak at $\xi_{STBL} = -0.14$:

$$\left.\left(\frac{(c_{N1}/c_{N2})+\xi_{\mathrm{STBL}}}{1/c_{N2}}\right)\right|_{\xi_{\mathrm{STBL}}=-0.14} = 0 \quad (14)$$

Normal distribution $\sigma = 0.14$:

$$\left.\left(\frac{(c_{N1}/c_{N2})+\xi_{\mathrm{STBL}}}{1/c_{N2}}\right)\right|_{\xi_{\mathrm{STBL}}=0} = 1 \quad (15)$$

$$c_{N1} = 1.0 \quad (16)$$

$$c_{N2} = \frac{1}{0.14} = 7.1 \quad (17)$$

The superposition of the point-symmetric and asymmetric model results in the new model for the yaw moment:

$$N_{SS} = \frac{1}{2}\rho V^2 \frac{\nabla_{\mathrm{STBL}}}{y_{cb}} \left(\frac{T_{SS}}{B_{SS}}\right)^{c_T} \left(c_{N_{sym}} \sin(\pi\xi_{\mathrm{STBL}}) e^{-\xi_{\mathrm{STBL}}^2} + c_{N_{asym}} e^{-(1.0+7.1\xi_{\mathrm{STBL}})^2}\right) \quad (18)$$

Fig. 33 shows the experimental values for one test condition along with the modelled results. Table 7 gives the properties of Eq. 18. It is noteworthy that the regression coefficient, $R^2=0.986$, is even higher for the yaw moment than for the surge and sway forces but the model contains one coefficient more.

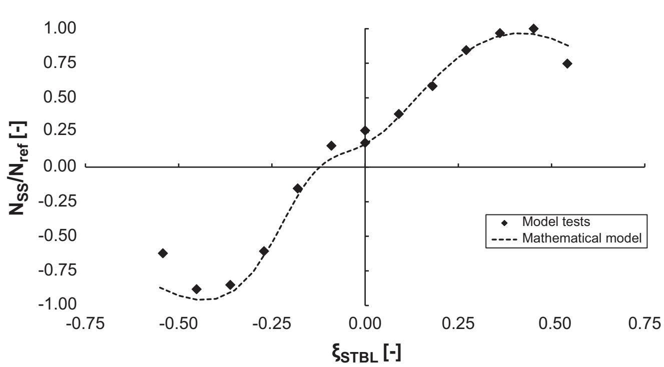

Fig. 33. The mathematical model for the yaw moment for a wide range of relative longitudinal positions between both vessels and with $y_{bb}=10.0$ m at 4.0 knots full scale and a water depth of 35.6 m.

Table 7
Parameter estimates for the mathematical model of the yaw moment on the service ship.

Parameter	Estimate	Std. error/ estimate	95% confidence interval	
			Lower bound/ estimate	Upper bound/ estimate
$C_{N_{sym}}$	$0<C_{N_{max}}<1$	0.04	0.92	1.07
C_T	$0<C_T<10$	0.02	0.97	1.03
$C_{N_{asym}}$	$0<C_{N_{asym}}<1$	0.06	0.89	1.12

R^2 squared = 1 − (residual sum of squares)/(corrected sum of squares) = 0.986.

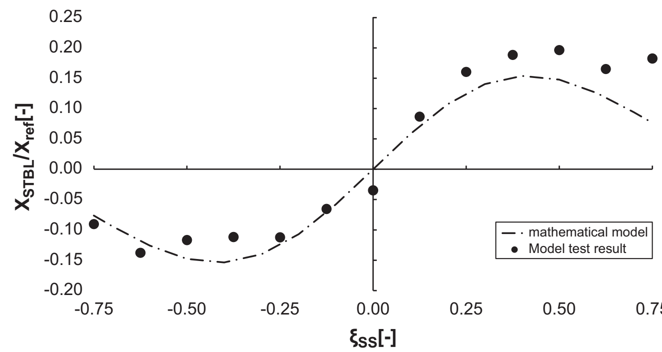

Fig. 34. Comparison between the measured surge force and the result of the mathematical model for a wide range of relative longitudinal positions between both vessels and with $y_{bb}=10.0$ m at 4.0 knots full scale and a water depth of 35.6 m.

Table 8
Parameter estimates for the mathematical model of the surge force on the STBL.

Parameter	Estimate	Std. error/ estimate	95% confidence interval	
			Lower bound/ estimate	Upper bound/ estimate
$C_{X_{max}}$	$0<C_{X_{max}}<10$	0.01	0.97	1.03
C_T	$0<C_T<10$	0.45	0.12	1.88
C_Y	$0<C_Y<1$	0.28	0.45	1.56

R^2 = 1 − (residual sum of squares)/(corrected sum of squares) = 0.841.

4.2. Forces and moment on the STBL X_{STBL}, Y_{STBL}, N_{STBL}

The equations proposed for the surge force, sway force and the yaw moment induced by the STBL on the service ship will now be applied (with new coefficients) for the forces and moment induced by the service ship on the STBL.

4.2.1. Surge force X_{STBL}

Because of the conservation of energy it can be expected when the surge force of the service ship increases the surge force of the STBL will decrease and vice versa.

This expectation is confirmed in Fig. 34. An increase of the surge force of the STBL happens simultaneously with a decrease of the surge force of the service ship and vice versa. When Eq. 6 is made fit for the STBL it results in Eq. 19 and Table 8:

$$X_{\mathrm{STBL}} = c_{X_{max}} \frac{1}{2}\rho V^2 \frac{\nabla_{SS}}{Lpp_{\mathrm{STBL}}} \left(\frac{T_{\mathrm{STBL}}}{B_{\mathrm{STBL}}}\right)^{c_T} \left(\frac{B_{\mathrm{STBL}}}{y_{cb}}\right)^{c_y} \sin(\pi\xi_{SS}) e^{-\xi_{SS}^2} \quad (19)$$

Fig. 35 shows the mathematical model for the surge force for the service ship and the STBL for a wide range of relative longitudinal positions (ξ_{STBL} for the service ship and ξ_{SS} for the

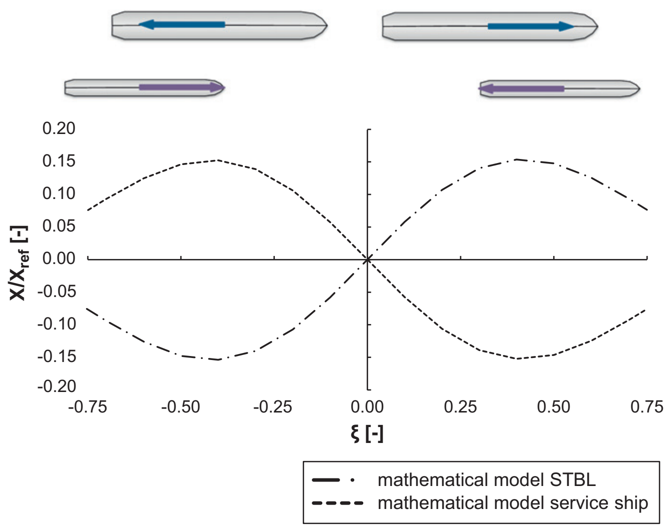

Fig. 35. Comparison between the modelled surge force for the STBL and the service ship (made dimensionless with the same X_{ref}) for a range of relative longitudinal positions.

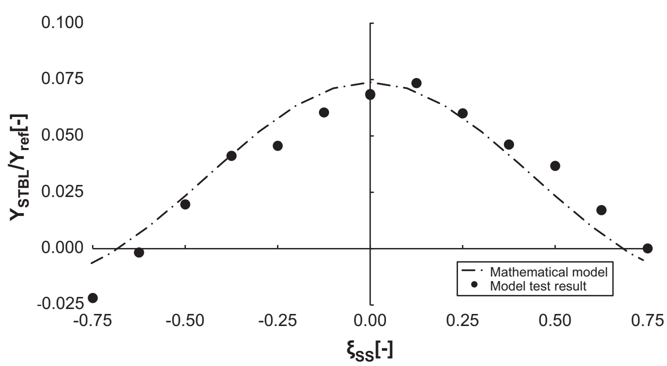

Fig. 36. Comparison between the measured sway force and the result of the mathematical model for a wide range of relative longitudinal positions between both vessels and with $y_{bb}=10.0$ m at 4.0 knots full scale and a water depth of 35.6 m.

ship to be lightered). Both are made dimensionless with the same (positive) X_{ref}. When the service ship is pushed forward by the proximity of the STBL, the STBL will be pulled back by the proximity of the service ship.

4.2.2. Sway force Y_{STBL}

The higher water velocities in between both vessels results in an attraction force of the service ship towards the STBL but also in an attraction force of the STBL towards the service ship (Fig. 36). Again this sway force peaks when both midships are at about the same relative longitudinal position. Similar as for the service ship, cf. Eq. 9, the sway force on the STBL is mathematically modelled with:

$$Y_{\mathrm{STBL}} = c_{Y_{\max}} \frac{1}{2}\rho V^2 \frac{\nabla_{SS}}{Lpp_{\mathrm{STBL}}} \left(\frac{T_{\mathrm{STBL}}}{B_{\mathrm{STBL}}}\right)^{c_T} \left(\frac{B_{\mathrm{STBL}}}{y_{cb}}\right)^{c_y} \cos(c_\xi \pi \xi_{SS}) e^{-\xi_{SS}^2} \quad (20)$$

Fig. 36 compares the experimental values with the modelled results and Table 9 gives the properties of Eq. 20.

As can be seen in Fig. 36 the sway force on the STBL does not change from attraction to a repulsion force for ξ_{SS}-values around 0.40. Therefore the coefficient c_ξ is different from and lower than one. Both ships are attracted to each other for all relative longitudinal positions as they occur during a standard lightering manoeuvre, as shown in Fig. 37.

Table 9
Parameter estimates for the mathematical model of the sway force on the STBL.

Parameter	Estimate	Std. error/ estimate	95% confidence interval	
			Lower bound/ estimate	Upper bound/ estimate
$C_{Y_{max}}$	$0<C_{Y_{max}}<10$	0.03	0.94	1.06
C_T	1	NA	NA	NA
C_Y	$0<C_Y<10$	0.05	0.90	1.10
C_ξ	$0<C_\xi<1$	0.02	0.96	1.04

$R^2=1-$(residual sum of squares)/(corrected sum of squares)$=0.886$.

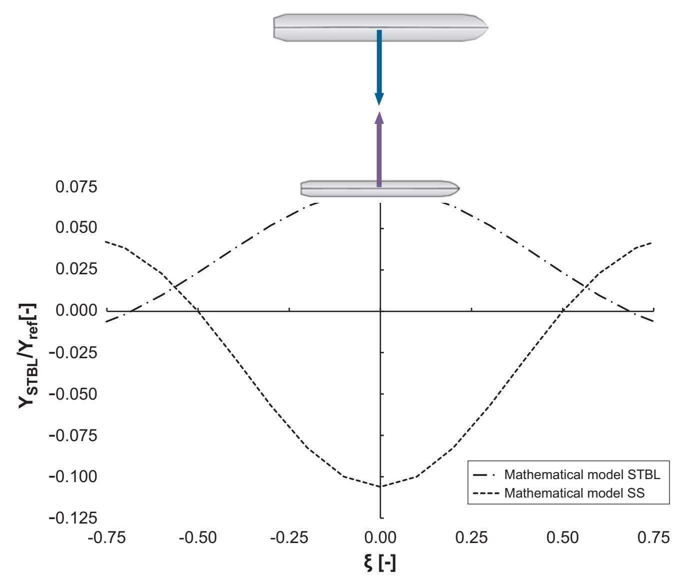

Fig. 37. Comparison between the modelled sway force for the STBL and the service ship (made dimensionless with the same Y_{ref}) for a range of relative longitudinal positions.

4.2.3. Yaw moment N_{STBL}

When the midship section of the STBL is ahead of the midship section of the service ship the yaw moment will be directed so that her bow is pushed away from the service ship and her stern attracted towards the service ship and the other way around. The bow away moment at very small ξ_{SS} values is much less present than for the service ship. For reasons of consistency the asymmetric part of the model is remained and the yaw moment on the STBL is modelled as:

$$N_{\mathrm{STBL}} = \frac{1}{2}\rho V^2 \frac{\nabla_{SS}}{y_{cb}} \left(\frac{T_{\mathrm{STBL}}}{B_{\mathrm{STBL}}}\right)^{c_T} (c_{N_{sym}} \sin(\pi\xi_{SS}) e^{-\xi_{SS}^2} + c_{N_{asym}} \times e^{-(1+5.2\xi_{SS})^2}) \quad (21)$$

Fig. 38 compares the experimental values with the modelled results for one test condition and Table 10 gives the properties of Eq. 21. Fig. 39 demonstrates that the yaw moment of the STBL is directed with the bow away from the service ship when the latter sails with the midship aft of the STBL's midship. At the same relative position, the yaw moment of the service ship is directed with her bow towards the STBL. When the service ship sails with the midship ahead of the STBL's midship, the yawing moment on both ships changes its sign. When the relative longitudinal position ξ is close to zero (as is the case in a standard lightering manoeuvre) the yaw moment of the STBL is relatively small and directed with her bow away from the service ship. The yaw

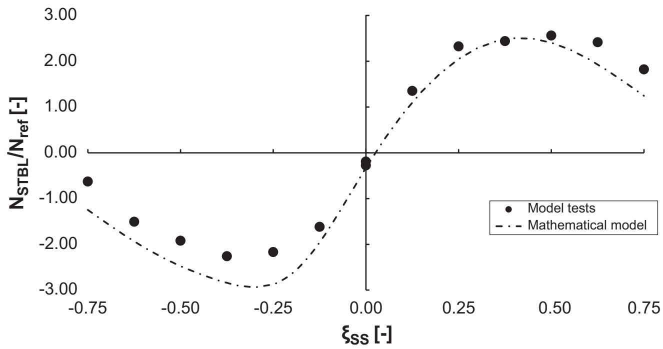

Fig. 38. Comparison between the measured yaw moment and the result of the mathematical model for a wide range of relative longitudinal positions between both vessels and with $y_{bb}=10.0$ m at 4.0 knots full scale and a water depth of 35.6 m.

Table 10
Parameter estimates for the mathematical model of the yaw moment on the STBL.

Parameter	Estimate	Std. error/ estimate	95% confidence interval	
			Lower bound/ estimate	Upper bound/ estimate
C_T	$0<C_T<10$	0.03	0.95	1.05
$C_{N_{sym}}$	$0<C_{N_{sym}}<10$	0.07	0.87	1.13
$C_{N_{asym}}$	$-10<C_{N_{asym}}i<0$	-0.12	1.24	0.75

$R^2=1-$(residual sum of squares)/(corrected sum of squares)$=0.970$.

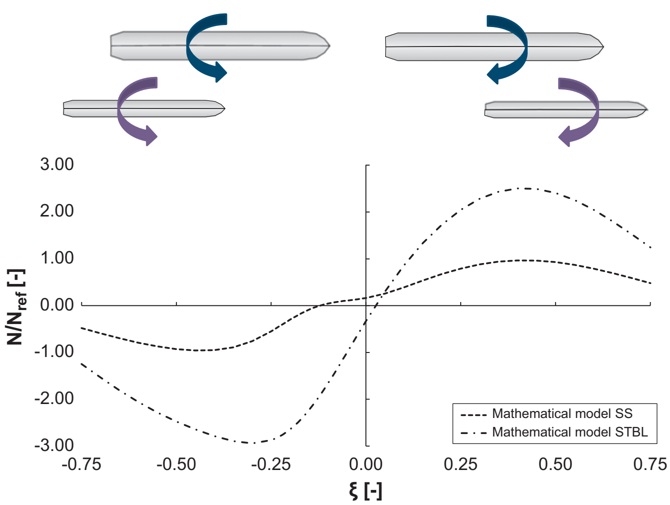

Fig. 39. Comparison between the modelled yaw moment for the STBL and the service ship (made dimensionless with the same N_{ref}) for a range of relative longitudinal positions.

moment of the service ship is in this position also directed with her bow away from the STBL.

4.3. General lightering formulae

Overall the formula for the longitudinal force X, lateral force Y and yaw moment N induced by a target ship (suffix T) on the own ship (suffix O) when both sail at the same forward speed can be summarised with:

$$X_O = c_{X_{max}} \frac{1}{2}\rho V^2 \frac{\nabla_T}{Lpp_O}\left(\frac{T_O}{B_O}\right)^{c_T}\left(\frac{B_O}{y_{c_O b_T}}\right)^{c_y} \sin(\pi\xi_T)e^{-\xi_T{}^2} \quad (22)$$

$$Y_O = c_{Y_{max}} \frac{1}{2}\rho V^2 \frac{\nabla_T}{Lpp_O}\left(\frac{T_O}{B_O}\right)^{c_T}\left(\frac{B_O}{y_{c_O b_T}}\right)^{c_y} \cos(c_\xi \pi\xi_T)e^{-\xi_T{}^2} \quad (23)$$

$$N_O = \frac{1}{2}\rho V^2 \frac{\nabla_T}{y_{c_O b_T}}\left(\frac{T_O}{B_O}\right)^{c_T}(c_{N_{sym}} \sin(\pi\xi_T)e^{-\xi_T{}^2} + c_{N_{asym}} \times e^{-(1+c_{N_2}\xi_T)^2}) \quad (24)$$

5. Conclusions

The current article provided an extensive analysis of the model tests on lightering described in Lataire et al. (2009a). The influence of the relative longitudinal and lateral position between the ships as well as forward speed, displacement of the vessels and water depth on the hydrodynamic ship-to-ship interaction effects – more particularly surge force X, sway force Y and yaw moment N – have been investigated.

A relative longitudinal separation between both ships induces a surge force trying to reduce this separation, meaning that the most forward positioned ship is pulled back while the other ship is pushed forward. The magnitude of the surge force increases when both ships are laterally positioned closer to each other, with a higher forward speed and with a higher displacement of the target ship.

The sway force peaks when both midships are at the same longitudinal position and is directed as an attraction force for both ships, however, this is only the case for deep water. This attraction force increases with decreasing lateral position between both ships, increasing forward speed and with a higher displacement of the target ship.

When the stern of the own ship is ahead of the target ship a yaw moment is induced, attracting the bow of the own ship towards the target ship. The induced yaw moment on the target ship in this position will be directed with the bow away from the own ship. The magnitude of the yaw moment increases with a decreasing lateral position between both ships, increasing forward speed and a higher displacement of the target ship. When both midship sections are positioned at the same relative longitudinal position a small but important yaw moment attempts to attract the ships' sterns to each other.

The analysis of the experimental results has been used to propose a new mathematical model specifically adapted for lightering operations with both ships advancing at the same forward speed in deep water. The model proposes equations for the surge and sway force and the yaw moment on the service ship and on the ship to be lightered. Particular attention has been paid to accurately modelling the most important conditions for lightering operations, notably at close to zero stagger distance between the ships.

The agreement between the equations and the experimental values is good, with only a limited number of coefficients, which allows an easy implementation in a ship manoeuvring simulator. Such a simulator can now be used for training purposes. Although nowadays the lightering manoeuvre takes place in deep water only, the model can be extended in the future to cope with the influence of the (shallow) water depth on the lightering manoeuvre.

Acknowledgments

The project "KMB Investigating hydrodynamic aspect and control systems for ship-to-ship operations" is co-ordinated by MARINTEK (Trondheim, Norway) and financially supported by the Research Council of Norway. All model tests have been carried out at the towing tank for manoeuvres in shallow water (co-operation Flanders Hydraulics Research — Ghent University) in Antwerp, Belgium.

References

Chen, G.R., Fang, M.C., 2001. Hydrodynamic interactions between two ships advancing in waves. Ocean Eng. 28 (8), 1053–1078.

De Decker, B., 2006. Ship–ship interaction during lightering operations. Maritime Technology Division, Ghent University, M.Sc. Dissertation.

Fang, M. C., Chen, G.R., 2003. The effect of clearance and speed on the relative motions between two ships advancing in waves. In: Proceedings of the 13th International Offshore and Polar Engineering Conference, Honolulu, Hawaii, USA, pp. 552–557.

Fang, M.C., Kim, C.H., 1986. Hydrodynamically coupled motions of two ships advancing in oblique waves. J. Ship Res. 30 (3), 159–171.

Husjord, D., Øritsland,T.A., Pedersen, E., 2011. Integration and testing of an STS decision support system in a full-mission ship maneuvering simulator. In: Proceedings of the Second International Conference on Ship Manoeuvring in Shallow and Confined Water: Ship to Ship Interaction, Trondheim, Norway: pp. 183–192.

Hayden, C., 2011. Invited keynote speech: ship to ship transfers – a global perspective. In: Proceedings of the Second International Conferenceon Ship Manoeuvring in Shallow and Confined Water: Ship to Ship Interaction, Trondheim, Norway. pp. 13–30.

Lataire, E., Vantorre, M., Delefortrie, G., 2009a. Captive model testing for ship to ship operations. In: MARSIM '09 Conference Proceedings, Panama City, Panama, pp. M-14-1/10.

Lataire, E., Vantorre, M. and Eloot, K., 2009b. Systematic model tests on ship–bank interaction effects. In: Proceedings of the First International Conference on Ship Manoeuvring in Shallow and Confined Water: Bank Effects, Antwerp, Belgium, pp. 9–22.

Lataire, E., Vantorre, M., Vandenbroucke, J. and Eloot, K., 2011. Ship to ship interaction forces during lightering operations. In: Proceedings of the Second International Conference on Ship Manoeuvring in Shallow and Confined Water: Ship to Ship Interaction, Trondheim, Norway, pp. 211–221.

Opheim, O. K., 2005. Experimental investigation of ship to ship interaction in lightering operations. NTNU, Project Thesis.

Pedersen, E., Shimizu, E, Berg, T.E., 2008. On the development of guidance system design for ships operating in close proximity. In: IEEE PLANS. Position Location and Navigation Symposium, Monterey, Ca, USA, pp. 966–971.

Sakakibara, S., Yamada, S., Shimizu, E., Okuyama, E. and Oda, H., 2011. Advanced ship manoeuvring and mooring support system at ship-to-ship transfer operations by fender monitoring system of pneumatic fenders. In: Proceedings of the Second International Conference on Ship Manoeuvring in Shallow and Confined Water: Ship to Ship Interaction, Trondheim, Norway, pp. 309–314.

Shimizu, E., Pedersen, E., 2011. Relative distances and speeds measurement system for STS lightering operations using stereo-cameras. In: Proceedings of the Second International Conference on Ship Manoeuvring in Shallow and Confined Water: Ship to Ship Interaction, Trondheim, Norway, pp. 315–318.

SIMMAN 2008, Workshop on Verification and Validation of Ship Manoeuvring Simulation Methods, Copenhagen, Denmark, April 14–16 2008 〈www.simman 2008.dk〉.

Skejic, R., Berg, T.E., 2009. Hydrodynamic interaction effects during lightering operation in calm water — theoretical aspects. In: MARSIM '09 Conference Proceedings, Panama City, Panama, pp. M-8-1/9.

Skejic, R., Berg, T.E., 2010. Combined seakeeping and maneuvering analysis of a two ship lightering operation. In: Proceedings of the 29th Annual International Conference on Offshore Mechanics and Arctic Engineering (OMAE 2010), Shanghai, China, Paper OMAE2010-20616.

Skejic, R., Faltinsen, O.M., 2007. A unified seakeeping and maneuvering analysis of two interacting ships. Second International Conference on Marine Research and Transportation, Ischia, Italy, pp. 209–218.

Stern, F.; Agdrup, K. (Ed.) (2008). SIMMAN 2008. Workshop on Verification and Validation of Ship Manoeuvring Simulation Methods, Copenhagen, April 14–16 2008: Preprints of Workshop Proceedings: Volume 1. Summary, Test Cases, Methods and Papers. Force Technology: Brøndby.

Tuck, E.O., Newman, J.N., 1974. Hydrodynamic interactions between ships. In: Tenth Symposium on Naval Hydrodynamics. Cambridge, Ma, USA, pp. 35-70.

Van Kerkhove, G., Vantorre, M., Delefortrie, G. 2009. Advanced model testing techniques for ship behaviour in shallow and confined water. Proceedings of AMT 2009 (The First International Conference on Advanced Model Measurement Technology for the EU Maritime Industry), Nantes, France.

Vantorre, M., Verzhbitskaya, E., Laforce, E., 2002. Model test based formulations of ship–ship interaction forces. Ship Tech. Res. 49 (3), 124–141.

Xiang, X., Faltinsen, O.M., 2010. Maneuvering of two interacting ships in calm water. In: Eleventh International Symposium on Practical Design of Ships and Other Floating Structures. Rio de Janeiro, Brazil, pp. 161–171.

Yasukawa, H.,Yoshida, S., 2011. Hydrodynamic interaction of two thin ships with rudder in close proximity. In: Proceedings of the Second International Conference on Ship Manoeuvring in Shallow and Confined Water: Ship to Ship Interaction, Trondheim, Norway, pp. 399–406.